Quantum phase transitions and collapse of the Mott gap in the $d=1+\epsilon$ dimensional Hubbard model with $2k_F$ umklapp scattering

Jun-ichiro Kishine*
Department of Theoretical Studies, Institute for Molecular Science, Okazaki 444-8585, Japan
(Received 28 October 1999; revised manuscript received 29 March 2000)

We study the low-energy asymptotics of the $d=1+\epsilon$ dimensional Hubbard model with a circular Fermi surface where there is $2k_F$ umklapp scattering present *a priori*. Peculiarity of the $d=1+\epsilon$ dimensions is incorporated through the imbalance between the elementary particle-particle and particle-hole (PH) loops: infrared logarithmic singularity of the PH loop is smeared for $\epsilon>0$. The one-loop renormalization-group flows indicate that a quantum phase transition from a metallic phase to the Mott insulator phase occurs at a finite on-site Coulomb repulsion U for $\epsilon>0$. We also discuss effects of randomness.

I. INTRODUCTION

Correlation-driven metal-insulator transition (MIT) in the Hubbard model has been a basic problem in condensed-matter physics.[1] Central to this issue is the problem of quantum fluctuation controlled by the on-site Coulomb repulsion U, the bandwidth W, and the carrier concentration n. In the half-filled ($n=1$) case, the zero-temperature bandwidth control MIT occurs at a critical ratio of $\bar{U}=U/W$, $\bar{U}_c$. The exact solution of the Hubbard model is available only in the $d=1$ dimension, where the half-filled ground state is always an insulator with a finite charge excitation gap (Mott gap) at $\bar{U}>\bar{U}_c=0$.[2] In $d=2$, it is believed that there exists a finite $\bar{U}_c$ except in the case of the perfect nesting where $\bar{U}_c=0$.[3] In the case of the $d=2$ half-filled Hubbard model with the nearest neighbor and the second-nearest-neighbor hoppings, a Monte Carlo simulation,[4] a Hartree-Fock approximation, and the Gutzwiller approximation[5] all indicate that $\bar{U}_c$ is finite. In $d=\infty$, the dynamical mean-field approach[6] implies that the quasiparticle spectral weight in the vicinity of the Fermi surface vanishes continuously as U approaches a critical value $\bar{U}_c\sim 1$ from below.[7] The filling control MIT, which occurs as the carrier concentration approaches half-filling, has also been extensively studied.[1]

In the $d=1$ Hubbard model at half-filling, low-energy asymptotics is also well understood in terms of the renormalization-group (RG) flow of two-particle scattering strengths, g_1, g_2, and g_3, which correspond to the backward, forward, and $2k_F$ umklapp scatterings, respectively.[8,9] The RG scheme in $d=1$ is based on infrared logarithmic singularities of elementary particle-particle (PP) and particle-hole (PH) loops that have the same magnitude and opposite signs. In this context, the source of the Mott gap is the umklapp scattering, which becomes a relevant perturbation for $U>0$. The RG flow also indicates that the charge stiffness reaches zero during the renormalization process and the system becomes an insulator. Thus, the RG-based scenario is in perfect agreement with the exact solution.

Dimensionality effects on the $d=1$ Mott insulator phase were phenomenologically treated by cutting off either of the PP or the PH loops below some characteristic temperature.[10,11] In the case of weakly-coupled chains, dimensional crossovers caused by an interchain hopping $t_\perp$ have been studied by treating $t_\perp$ perturbatively and assuming that the scaling procedure in the one-dimensional regime at high-energy scales ($\omega\gg t_\perp$) remains valid down to the crossover energy scales.[12–14] Recently, the filling control MIT in coupled Hubbard chains with infinitely large coordination numbers was also studied.[15] However, these attempts have not clarified the dimensionality effects on the Mott gap, because feedback effects of the interchain processes on the Mott gap have been missing.

The RG method is straightforwardly extended to the case of $d=1+\epsilon$ ($0<\epsilon\ll 1$) dimensions.[16] In this case, only the PP loop remains logarithmically singular, while the PH loop is smeared for $\epsilon>0$.[17] By taking this fact into account from the beginning of renormalization processes, the feedback effects on the Mott gap may be incorporated. In this paper, by using the one-loop RG method, we examine dimensionality effects on the RG flow of the umklapp process and discuss possible QPT's in the Hubbard model with a circular Fermi surface in $d=1+\epsilon$ dimensions.

If randomness exists, a QPT between the Mott insulator and a randomness-driven Anderson insulator might arise. In the case of $d=1$ at half-filling, based on the RG method, Fujimoto and Kawakami[18] found that sufficiently strong random forward scattering destroys the Mott gap. Recently, Ohtsuka *et al.*[19,20] studied the half-filled Hubbard model containing site randomness by using the quantum Monte Carlo technique and found that the strong randomness destroys the Mott gap. In this paper, we also discuss randomness effects on the QPT's.

This paper is organized as follows: In Sec. II we introduce the g-ology effective action, derive the one-loop RG equations, and discuss possible QPT's in the absence of randomness. The effects of randomness are discussed in Sec. III, followed by concluding remarks in Sec. IV.

II. HUBBARD MODEL IN $D=1+\epsilon$ DIMENSIONS

In this section, we study interplay of electron correlation and dimensionality effects in the Hubbard model with a circular Fermi surface in $d=1+\epsilon$ dimensions, where there is $2k_F$ umklapp scattering.

A. Effective action

We start with the effective action,

$$S_{\rm Hubbard}=\sum_{\sigma}\int_{-\infty}^{\infty}\frac{d\varepsilon}{2\pi}\int\frac{d^d\boldsymbol{k}}{(2\pi)^d}\mathcal{G}^{-1}(\boldsymbol{k},i\varepsilon)c_\sigma^*(K)c_\sigma(K)$$
$$-\frac{\pi v_F}{2}\sum_{\sigma,\sigma'}\prod_{i=1}^{4}\int_{-\infty}^{\infty}\frac{d\varepsilon_i}{2\pi}\int\frac{d^d\boldsymbol{k}_i}{(2\pi)^d}$$
$$\times\delta(\varepsilon_4+\varepsilon_3-\varepsilon_2-\varepsilon_1)$$
$$\times\delta(\boldsymbol{k}_4+\boldsymbol{k}_3-\boldsymbol{k}_2-\boldsymbol{k}_1-\boldsymbol{G})g^{\sigma\sigma'}_{\boldsymbol{k}_1,\boldsymbol{k}_2,\boldsymbol{k}_3}$$
$$\times c_\sigma^*(K_4)c_{\sigma'}^*(K_3)c_{\sigma'}(K_2)c_\sigma(K_1), \tag{1}$$

where $c_\sigma^*(K)$ and $c_\sigma(K)$ are the Grassmann variables representing the electron with the spin σ and $K=(\boldsymbol{k},\varepsilon)$ with $\boldsymbol{k}$ and ε being a d-dimensional momentum and a Fermion thermal frequency, respectively. The noninteracting one-particle propagator is given by

$$\mathcal{G}^{-1}(\boldsymbol{k},i\varepsilon)=i\varepsilon-\xi(\boldsymbol{k}). \tag{2}$$

The one-particle dispersion is $\xi(\boldsymbol{k})=(\boldsymbol{k}^2-k_F^2)/2m$ and the Fermi surface is a d-dimensional sphere $|\boldsymbol{k}|=k_F$. Since we consider only the energy scale that is much smaller than the Fermi energy, we linearize one-particle dispersion as

$$\xi(\boldsymbol{k})=v_F(|\boldsymbol{k}|-k_F), \tag{3}$$

where v_F is the Fermi velocity. The bandwidth cutoff E_0 is introduced and the one-particle processes are restricted to $-E_0\leqslant\xi(\boldsymbol{k})\leqslant E_0$. In the two-particle scattering part of $S_{\rm Hubbard}$, $|\boldsymbol{G}|=0$ and $|\boldsymbol{G}|=4k_F$ for the normal and the $2k_F$ umklapp processes, respectively. Although the lattice structure in $d=1+\epsilon$ is not directly involved in this paper, we here assume that there is the $2k_F$ umklapp scattering present *a priori*. We also assume that the normal scattering processes that enter the RG equations in $d=1+\epsilon$ are, as in the case of $d=1$, the backward scattering with large momentum transfer $|\boldsymbol{k}_3-\boldsymbol{k}_2|\sim 2k_F$ and the forward scattering with small momentum transfer $|\boldsymbol{k}_3-\boldsymbol{k}_2|\sim 0$. Dimensionless scattering strengths for the scattering processes considered here are denoted by g_1 [backward], g_2 [forward], and g_3 [$2k_F$ umklapp]. The corresponding scattering vertices are shown in Figs. 1(a)–1(c), respectively, where the momentum transfer between the solid and dashed lines is $2k_F$ in magnitude [the solid and dashed lines here correspond to the right- and left-moving one-particle propagators in the $d=1$ limit]. Unrenormalized scattering strengths are related to the on-site Coulomb repulsion U as[9]

$$g_{1;0}=g_{2;0}=g_{3;0}=U/\pi v_F\equiv\tilde{U}. \tag{4}$$

Restriction of the momentum transfer in the normal scattering procceses to $|\boldsymbol{k}_3-\boldsymbol{k}_2|\sim 2k_F$ and 0 in $d=1+\epsilon$ may be justified, by approaching the limit $d=1$ from $d=2$ in the following way. In the case of $d=2$ circular Fermi surface, there are three distinct types of low-energy normal scattering process:[17] forward (F) scattering [$\boldsymbol{k}_1=\boldsymbol{k}_4$, $\boldsymbol{k}_2=\boldsymbol{k}_3$], exchange (E) scattering [$\boldsymbol{k}_1=\boldsymbol{k}_3$, $\boldsymbol{k}_2=\boldsymbol{k}_4$], and Cooper ($C$) scattering [$\boldsymbol{k}_1+\boldsymbol{k}_2=0$]. F and E scattering can be parametrized by the angle ϕ between $\boldsymbol{k}_1$ and $\boldsymbol{k}_2$ as $g_{\rm F}(\phi)$ and $g_{\rm E}(\phi)$, respectively, while C scattering is parametrized by the angle ϕ between $\boldsymbol{k}_1$ and $\boldsymbol{k}_4$ as $g_{\rm C}(\phi)$. Then, the actions for these scattering processes in $d=1+\epsilon$ contain integration over these specific angles with the measure proportional to $\mathcal{M}_\epsilon(\phi)=\epsilon/(\sin\phi)^{1-\epsilon}$ [see Eq. (5) and note $S_\epsilon\sim\epsilon$]. In Fig. 1(d), we show ϕ dependence of $\mathcal{M}_\epsilon(\phi)$ for $\epsilon=0.01$, 0.1, and 0.5. We see that $\mathcal{M}_\epsilon(\phi)$ has peaks at $\phi=0$ and π for $\epsilon\ll 1$ [$\mathcal{M}_\epsilon(\phi)\to\delta(\phi)+\delta(\phi-\pi)$ for $\epsilon\to 0$]. Consequently, the one-dimensional g-ology classification may be valid even in $d=1+\epsilon$ with the correspondence[21] $g_{\rm F}(0)=g_4$, $g_{\rm F}(\pi)=g_2$, $g_{\rm E}(0)=g_4$, $g_{\rm E}(\pi)=g_1$, $g_{\rm C}(0)=g_2$, and $g_{\rm C}(\pi)=g_1$. We here neglect the g_4 process that does not enter the one-loop RG equations discussed below.

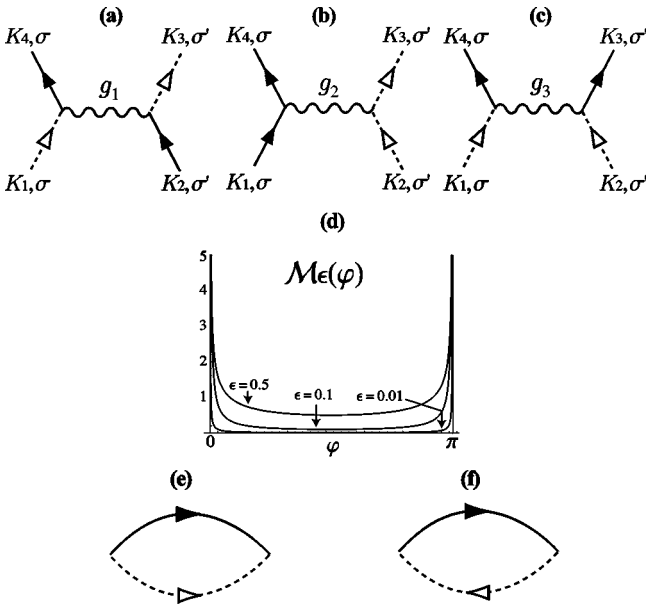

FIG. 1. Two-particle scattering vertices for the (a) backward, (b) forward, and (c) $2k_F$ umklapp scattering processes. The momentum transfer between the solid and dashed lines is $2k_F$ in magnitude. (d) ϕ dependence of $\mathcal{M}_\epsilon(\phi)$ for $\epsilon=0.01$, 0.1, and 0.5. The elementary (e) particle-particle (PP) and (f) $2k_F$ particle-hole (PH) loops.

B. The elementary particle-particle and particle-hole loops

The peculiarity of $d=1+\epsilon$ dimensions is incorporated only through the integration measure,

$$\int d^d\boldsymbol{k}/(2\pi)^d.$$

For our purpose here, it is sufficient to integrate over $k=|\boldsymbol{k}|$ and the angle θ spanned by $\boldsymbol{k}$ and another fixed momentum. Then we can use[22]

$$\int\frac{d^d\boldsymbol{k}}{(2\pi)^d}(\cdots)=\frac{S_{d-1}}{(2\pi)^d}\int k^{d-1}dk\int_0^\pi d\theta(\sin\theta)^{d-2}(\cdots), \tag{5}$$

where $S_d=2\pi^{d/2}/\Gamma(d/2)$ is the surface area of the d-dimensional unit sphere.

As is well known, in any dimension, the real part of the elementary PP loop [Fig. 1(e)] at the zero total momentum,

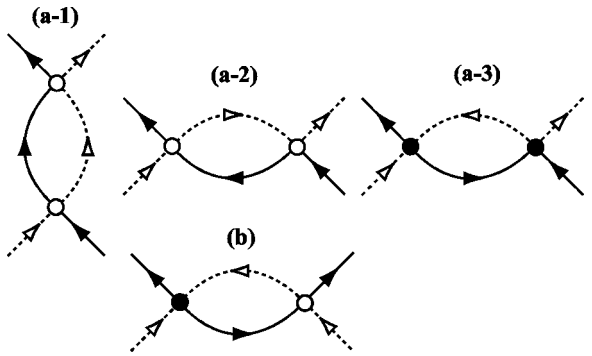

FIG. 2. Vertex correction diagrams for the (a) normal $[g_1, g_2]$ and (b) umklapp $[g_3]$ processes. White and black circles represent the normal and umklapp scatterings, respectively.

$$\Delta_0(\omega)=\int \frac{d^d\boldsymbol{k}}{(2\pi)^d}\frac{\Theta(\xi_{-\boldsymbol{k}})-\Theta(-\xi_{\boldsymbol{k}})}{\omega-\xi_{-\boldsymbol{k}}-\xi_{\boldsymbol{k}}+i0^+}, \tag{6}$$

with $\Theta(x)$ being the step function, exhibits an infrared logarithmic singularity of the form[16,17]

$$\Re\Delta_0(\omega)=-\frac{S_d}{(2\pi)^d}\frac{k_F^{d-1}}{v_F}\log(\omega/E_0). \tag{7}$$

In $d=1+\epsilon$, we obtain

$$\Re\Delta_0(\omega)\sim-\frac{1}{2\pi v_F}\log(\omega/E_0), \tag{8}$$

which exactly reproduces the result in $d=1$.

On the other hand, the real part of the elementary PH loop at $2k_F$ momentum transfer [Fig. 1(f)],

$$\Pi_{2k_F}(\omega)=\int \frac{d^d\boldsymbol{k}}{(2\pi)^d}\frac{\Theta(\xi_{\boldsymbol{k}+\boldsymbol{Q}})-\Theta(\xi_{\boldsymbol{k}})}{\omega-\xi_{\boldsymbol{k}+\boldsymbol{Q}}+\xi_{\boldsymbol{k}}+i0^+}, \tag{9}$$

with $|\boldsymbol{Q}|=2k_F$, unlike the case of $d=1$, no longer exhibits an infrared singularity for $d>1$ and in $d=1+\epsilon$, takes the form

$$\Re\Pi_{2k_F}(\omega)\sim\frac{1}{2\pi v_F}\left[\frac{\tilde{\omega}^{\epsilon/2}}{\epsilon/2}+C_\epsilon\right], \tag{10}$$

where $\tilde{\omega}=\omega/2v_Fk_F$ and C_ϵ is a constant independent of ω. Although this form has already been suggested in Ref. 16, we confirm, in the appendix, that the ω-dependent term in Eq. (10) is uniquely determined.

C. One-loop renormalization

One-loop renormalization of the scattering strengths comes from the vertex correction diagrams represented in Figs. 2(a) and 2(b) for the normal $[g_1, g_2]$ and umklapp $[g_3]$ processes, respectively. The renormalized scattering strength, g_1', g_2', and g_3', are thus given by

$$g_1'=g_1+g_1g_2\ln\frac{\omega}{E_0}-(g_2-g_1)g_1\pi(\omega), \tag{11}$$

$$g_2'=g_2+\frac{1}{2}(g_1^2+g_2^2)\ln\frac{\omega}{E_0}-\frac{1}{2}(g_2^2+g_3^2)\pi(\omega), \tag{12}$$

$$g_3'=g_3+g_3(g_1-2g_2)\pi(\omega), \tag{13}$$

where $\pi(\omega)=2\pi v_F\Re\Pi_{2k_F}(\omega)$. Figure 2(a1) contains the PP loop and all other diagrams contain the PH loop. In particular, renormalization of the umklapp process comes from the PH loop only. By differentiating Eqs. (11)-(13) with respect to the scaling parameter

$$l=\ln(E_0/\omega), \tag{14}$$

we obtain the RG equations

$$\frac{dg_1}{dl}=-g_1g_2+(g_2-g_1)g_1\lambda_l, \tag{15}$$

$$\frac{dg_2}{dl}=-(g_1^2+g_2^2)/2+(g_2^2+g_3^2)\lambda_l/2, \tag{16}$$

$$\frac{dg_3}{dl}=-g_3(g_1-2g_2)\lambda_l. \tag{17}$$

The PH loop gives rise to the smooth cutoff,[16]

$$\lambda_l\equiv\left|\frac{\partial}{\partial l}\pi(\omega)\right|=\left(\frac{E_0}{2k_Fv_F}\right)^{\epsilon/2}\exp[-\epsilon l/2]\sim\exp[-\epsilon l/2], \tag{18}$$

where the ratio of the two cutoff energy scales $E_0/2k_Fv_F$ is of the order of unity. In the absence of the umklapp process, the RG equations obtained here reproduces those in Ref. 16.

D. Renormalization-group flow and QPT

In the $d=1$ half-filled Hubbard model, the charge degrees of freedom are governed by the combination of (g_3, $G=g_1-2g_2$) with the flow lines $(G-\text{const})^2-g_3^2=\text{const}$. For *any finite* $U>0$, they are scaled to $(g_3^*=\infty, G^*=-\infty)$, which implies the Mott gap opens due to the relevant umklapp scattering. This RG flow also indicates that the charge stiffness $K_\rho=\sqrt{(1+G)/(1-G)}$ reaches zero during the renormalization process and the system becomes an insulator. To complement this scenario, it is useful to map the charge sector of the $d=1$ half-filled Hubbard model onto the (1+1)-dimensional sine-Gordon model by using the bosonization technique. The sine Gordon action is of the form:[9]

$$S_{\rm SG}=\int d^2\boldsymbol{r}\{u_\rho/2\,[\nabla_{\boldsymbol{r}}\Psi_\rho(\boldsymbol{r})]^2-[2g_3/(\pi\alpha)^2]\cos[\sqrt{8\pi K_\rho}\Psi_\rho(\boldsymbol{r})]\},$$

where $\boldsymbol{r}=(x,\tau)$ represents (1+1)-dimensional space-time coordinates, $\Psi_\rho(\boldsymbol{r})$ represents a charge boson (holon) field, u_ρ is the holon velocity, and α is a short distance cutoff. By applying the RG method directory to the sine-Gordon model,[23] we obtain the RG equations $dg_3/dl=2(1-K_\rho)g_3$, and $dK_\rho/dl=-(8a\pi^2/\Xi_l^4)g_3^2K_\rho^3$, where

$$a=\int_0^1 d\rho\,\rho^3J_0(\rho)$$

and $\Xi_l=\Xi_0e^{-l}$ is the space-time cutoff. We thus see that g_3 becomes relevant for the initial condition $K_{\rho;0}<1$ [corre-

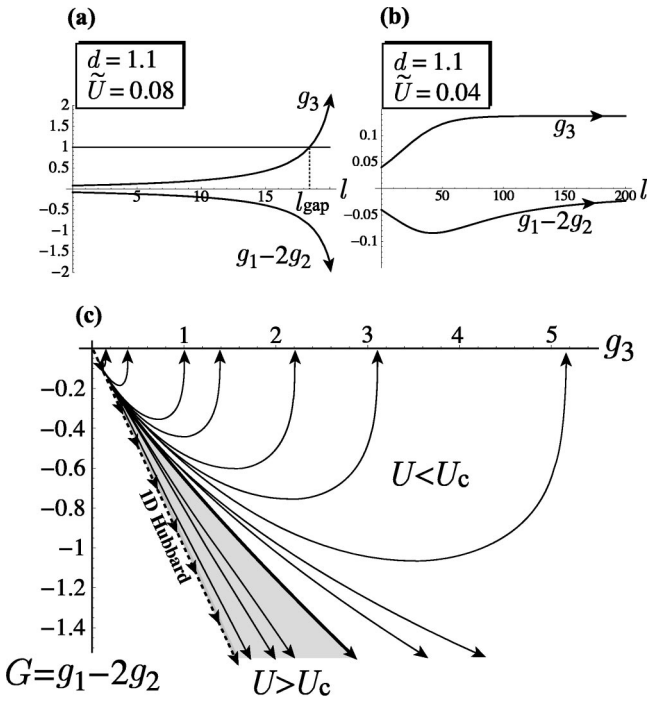

FIG. 3. RG flows in the case of $d=1.1$ with (a) $\tilde{U}=0.08$ and (b) 0.04. (c) The RG trajectories in terms of g_3 and $G=g_1-2g_2$ in $d=1.1$. A critical value is $\tilde{U}_c=0.0588$. In the $d=1$ half-filled Hubbard model, g_3 and G flow along the broken line denoted by ''1D Hubbard.''

sponding to $U>0$ for the Hubbard model] and then, accordingly, the charge stiffness K_ρ is scaled to zero.

Now we consider the case of $d=1+\epsilon$ dimensions. In Figs. 3(a) and 3(b) are shown the RG flows for $\tilde{U}=U/\pi v_F=0.08$ and 0.04, respectively, in $d=1.1$. In Fig. 3(c), we show the RG flows in terms of g_3 and $G=g_1-2g_2$ for various $\tilde{U}$ in $d=1.1$. It is found that there exists a critical value of $\tilde{U}$, $\tilde{U}_c=0.0588$. For $\tilde{U}>\tilde{U}_c$, the RG flows exhibit runaway trajectories toward $(g_3^*=\infty, G^*=-\infty)$ [shaded region in Fig. 3(c)], which implies the Mott gap opens at the low-energy limit just as in the case of $d=1$. The initial values of g_3 and G at $l=0$ correspond to the points on the line $G=-g_3$, represented by a broken line in Fig. 3(c). In the $d=1$ half-filled Hubbard model, g_3 and G flow along this line (denoted by ''1D Hubbard'') for any $U>0$.

On the other hand, the RG flows approach the fixed points, $(g_3^*=\text{const}, G^*=0)$ for $\tilde{U}<\tilde{U}_c$. Marginal behavior of g_3 is in accordance with $G=g_1-2g_2\to 0$ [see Eq. (17)] as $l\to\infty$. The smooth cutoff, $\lambda_l=\exp[-\epsilon l/2]$, in Eq. (17) causes suppression of g_3 during the renormalization process. This suppression becomes more conspicuous for larger ϵ. The fixed point $G^*=0$, corresponding to the noninteracting value of the charge stiffness, $K_\rho^*=1$, implies that the Mott gap collapses and the system becomes metallic at the low-energy limit. Thus a QPT from the metallic phase to the Mott insulator phase may occur at $\tilde{U}=\tilde{U}_c$.

Within the RG-based scheme, it remains debatable how the marginal behavior of g_3 for $\tilde{U}>\tilde{U}_c$ modifies the ground-state property. Regarding this point, recently the density-matrix renormalization group method was applied to three

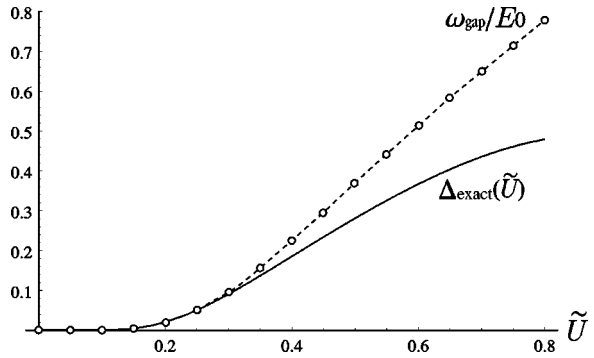

FIG. 4. $\tilde{U}$ dependence of $\Delta_{\text{exact}}(\tilde{U})$ and $\omega_{\text{gap}}=E_0e^{-l_{\text{gap}}}$ in $d=1$.

Hubbard chains coupled via the interchain one-particle hopping $t_\perp$.[24] As a result, it was found that the Mott gap decreases as $t_\perp$ increases. This numerical result strongly supports the RG-based view given here.

We here give qualitative discussion on the magnitude of the Mott gap based on the RG flows.[25] There is no tractable method to quantitatively obtain the magnitude of the Mott gap in $d>1$. However, the magnitude of the Mott gap is qualitatively given by the energy scale, $\omega_{\text{gap}}=E_0e^{-l_{\text{gap}}}$, at which the umklapp scattering strength exceeds unity, $g_3=1$ [see Fig. 3(a)].[13,14] To see how ω_{gap} reproduces the Mott gap, we compare the $\tilde{U}$ dependence of the exact Mott gap in $d=1$,[26]

$$\Delta_{\text{exact}}(\tilde{U})=\frac{2v_F}{\pi^2\tilde{U}^2}\int_1^\infty d\eta\,\frac{\sqrt{\eta^2-1}}{\sinh[\,\eta/\tilde{U}]}, \tag{19}$$

with that of ω_{gap} in $d=1$. There is arbitrariness in specification of the linearized bandwidth E_0. In Fig. 4, we show the case for $E_0=0.4v_F$, where ω_{gap} reproduces $\Delta_{\text{exact}}(\tilde{U})$ well at least for a weak $\tilde{U}$ where the weak-coupling RG scheme is valid.

In Fig. 5, we show a low-energy asymptotic phase dia-

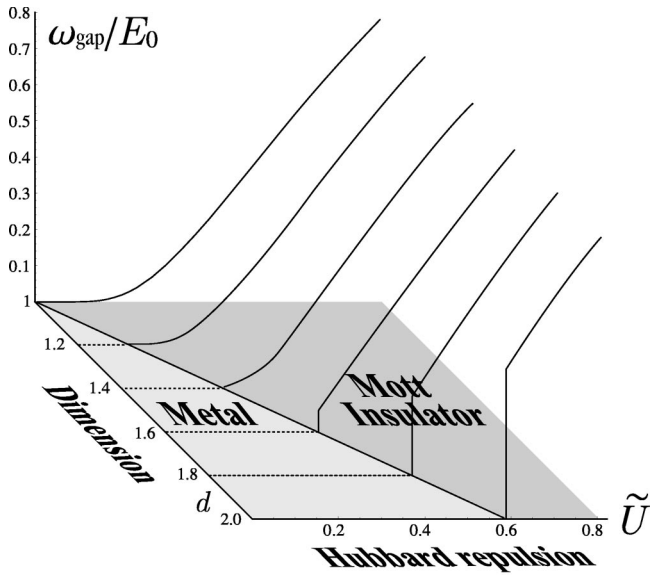

FIG. 5. A low-energy asymptotic phase diagram. We also show energy scales of the Mott gap, ω_{gap}/E_0, as a function of d and $\tilde{U}$.

gram. We also show $\omega_{\rm gap}/E_0$ as a function of d and $\tilde{U}$. For a fixed dimension, the low-energy asymptotic phase corresponds to a metal and the Mott insulator phases for $\tilde{P}<\tilde{U}_{\rm c}$ and $\tilde{U}>\tilde{U}_{\rm c}$, respectively. The critical value, $\tilde{U}_{\rm c}$, increases as d increases, suggesting a larger U is required for the Mott gap to open as the dimension increases. Accordingly, for a fixed $\tilde{U}$, $\omega_{\rm gap}/E_0$ decreases with increasing dimensions and disappears at some critical dimension, d_c [for example, $d_c=1.345$ for $\tilde{U}=0.2$].

Apparently $\omega_{\rm gap}/E_0$ grows continuously at $\tilde{U}=\tilde{U}_{\rm c}$ for $d\lesssim 1.4$. However, the transition is always discontinuous by the following reason. As is seen from Fig. 3(c), g_3 exceeds unity during the renormalization process and gives a finite value of $\omega_{\rm gap}/E_0$ even for $\tilde{U}<\tilde{U}_{\rm c}$. Nevertheless, $\omega_{\rm gap}/E_0$ has no physical interpretation for $\tilde{U}<\tilde{U}_{\rm c}$, since the charge stiffness is scaled to the noninteracting value. Therefore, $\omega_{\rm gap}/E_0$ grows discontinuously at $\tilde{U}=\tilde{U}_{\rm c}$. The magnitude of discontinuity at the transition point becomes more conspicuous as d increases. At present, it is not clear whether the discontinuity is an artifact of the one-loop RG method. To elaborate on this point would require the *two-loop* RG analysis, which is too involved a subject to be treated here.

We here comment on the relevance of the present study to the $d=2$ lattice Hubbard model. In this paper, we have studied only the case with a *circular* Fermi surface. Accordingly, our results are not smoothly connected to the $d=2$ square lattice Hubbard model. In particular, in the case of the perfect nesting, the van Hove singularity at $(\pm\pi,\pm\pi)$ points gives rise to the ''log-square'' singularity of the elementary PH loop at the momentum transfer $\boldsymbol{Q}=(\pi,\pi)$. Then the Hartree-Fock solution gives the gap[3] $\Delta\sim te^{-2\pi\sqrt{t/U}}$, which indicates that the ground state of the system is always an insulator for a finite U. This conclusion has been strongly supported by numerical studies.[1,3] However the possibility of the MIT at a finite U in the half-filled lattice Hubbard model with a Fermi surface of various geometries has been open to question. In the case of the $d=2$ half-filled Hubbard model with the nearest-neighbor and the second-nearest-neighbor hopping integrals (t and t', respectively), a Monte Carlo simulation,[4] a Hartree-Fock approximation, and the Gutzwiller approximation, including the antiferromagnetism[5] give finite critical values, $U/t=2.5$, 2.064, and 3.902, respectively, for $t'/t=0.2$. These results are consistent with the present findings that, *in the case of a circular Fermi surface, the MIT occurs at a finite U for* $\epsilon>0$.

III. EFFECTS OF RANDOMNESS

In this section, we study interplay of electron correlation, randomness, and dimensionality effects in the $d=1+\epsilon$ dimensional random Hubbard model with $2k_F$ umklapp scattering.[27]

A. Effective action for quenched randomness

The action for the scattering processes by the random potentials,

$$S_{\rm random}=-\sum_\sigma\int d^dx\int d\tau\, v(\boldsymbol{x})c_\sigma^*(\boldsymbol{x},\tau)c_\sigma(\boldsymbol{x},\tau)$$
$$=-\sum_\sigma\int\frac{d^dk}{(2\pi)^d}\int\frac{d^dq}{(2\pi)^d}\int d\tau\, v(\boldsymbol{q})$$
$$\times c_\sigma^*(\boldsymbol{k}+\boldsymbol{q},\tau)c_\sigma(\boldsymbol{k},\tau), \tag{20}$$

is added to the Hubbard action (1). Here,

$$c_\sigma(\boldsymbol{x},\tau)=\sum_{\boldsymbol{k}} e^{i\boldsymbol{k}\cdot\boldsymbol{x}}c_\sigma(\boldsymbol{k},\tau)$$

with τ being an imaginary time and

$$v(\boldsymbol{x})=\sum_{\boldsymbol{q}} e^{i\boldsymbol{q}\cdot\boldsymbol{x}}v(\boldsymbol{q})$$

is a random potential at the position $\boldsymbol{x}$. We assume that the random scattering processes that enter the RG equations in $d=1+\epsilon$ are, as in the case of $d=1$,[28] characterized by real and complex random fields $\eta(\boldsymbol{x})$ and $\xi(\boldsymbol{x})$ for the forward scattering with small momentum transfer $|\boldsymbol{q}|\sim 0$ and the backward scattering with large momentum transfer $|\boldsymbol{q}|\sim 2k_F$, respectively, due to the random potential. The random potentials are assumed to be governed by Gaussian distributions,

$$P_\eta\propto\exp\left[-D_\eta^{-1}\int d^dx\,\eta(\boldsymbol{x})^2\right], \tag{21}$$

$$P_\xi\propto\exp\left[-D_\xi^{-1}\int d^dx\,\xi(\boldsymbol{x})\xi^*(x)\right], \tag{22}$$

which lead to

$$\langle\eta(\boldsymbol{x})\eta(\boldsymbol{y})\rangle_{\rm random}=\frac{D_\eta}{2}\delta(\boldsymbol{x}-\boldsymbol{y}), \tag{23}$$

$$\langle\xi(\boldsymbol{x})\xi^*(\boldsymbol{y})\rangle_{\rm random}=\frac{D_\xi}{2}\delta(\boldsymbol{x}-\boldsymbol{y}), \tag{24}$$

where $D_\eta=(\pi N_F\tau_\eta)^{-1}$ and $D_\xi=(\pi N_F\tau_\xi)^{-1}$ with $\tau_{\eta,\xi}$ and N_F being the elastic-scattering mean free time and the one-particle density-of-states, respectively.

We consider the quenched randomness where averaging the free energy is accomplished by means of the replica trick, which is based on the identity

$$\ln Z=\lim_{N\to 0}\frac{Z^N-1}{N}. \tag{25}$$

We introduce N identical replicas of the system labeled by the index α. Then, by using the path-integral representation of the partition function, we have

$$Z^N=\int\prod_{\alpha=1}^N\mathcal{D}c^{\alpha *}\mathcal{D}c^\alpha\exp\left[\sum_{\alpha=1}^N S^\alpha\right], \tag{26}$$

where $S^\alpha=S^\alpha_{\rm Hubbard}+S^\alpha_{\rm random}$ is the total action and $\mathcal{D}$ symbolizes the measure over the fermionic Grassmann variables $c^{\alpha *}$ and c^α depending on a replica index α. The replica trick consists of performing the Gaussian ensemble average

$\langle Z^N\rangle_{\rm random}$ for integer N, continuing the result analytically to real N, and taking the limit $N\to 0$. We thus obtain

$$\langle Z^N\rangle_{\rm random}=\int d\eta\, P_\eta \int d\xi\, d\xi^* P_\xi \times\int\prod_{\alpha=1}^{N}\mathcal{D}c^{\alpha *}\mathcal{D}c^{\alpha}\exp\left[\sum_{\alpha=1}^{N}S^{\alpha}\right] \equiv\int\prod_{\alpha=1}^{N}\mathcal{D}c^{\alpha *}\mathcal{D}c^{\alpha}\exp\left[\sum_{\alpha=1}^{N}\tilde{S}^{\alpha}\right], \tag{27}$$

where the random scattering parts contained in $\tilde{S}^{\alpha}$ are given by[29]

$$\frac{D_\eta}{4}\sum_{\beta=1}^{N}\sum_{\sigma,\sigma'}\int d\tau_1\int d\tau_2\int\frac{d^d\mathbf{k}}{(2\pi)^d}\int\frac{d^d\mathbf{k}'}{(2\pi)^d} \times c_\sigma^{\alpha *}(\mathbf{k},\tau_1)c_\sigma^{\alpha}(\mathbf{k},\tau_1)c_{\sigma'}^{\beta *}(\mathbf{k}',\tau_2)c_{\sigma'}^{\beta}(\mathbf{k}',\tau_2) + \frac{D_\xi}{4}\sum_{\beta=1}^{N}\sum_{\sigma,\sigma'}\int d\tau_1\int d\tau_2\int\frac{d^d\mathbf{k}}{(2\pi)^d}\int\frac{d^d\mathbf{k}'}{(2\pi)^d} \times c_\sigma^{\alpha *}(\mathbf{k}+\mathbf{Q},\tau_1)c_\sigma^{\alpha}(\mathbf{k},\tau_1)c_{\sigma'}^{\beta *}(\mathbf{k}'-\mathbf{Q},\tau_2)c_{\sigma'}^{\beta}(\mathbf{k}',\tau_2),$$

where $|\mathbf{Q}|\sim 2k_F$.

We here change imaginary time variables τ_1 and τ_2 into $\Delta\tau=\tau_1-\tau_2$ and $\tau=(\tau_1+\tau_2)/2$. In the integration over $\Delta\tau$, we introduce a short distance cutoff Λ and keep only the region, $v_F|\Delta\tau|\leqslant\Lambda$, which couples the two-particle scattering processes and contributes to the RG equations. Then, the random forward-and backward-scattering parts are written as

$$\tilde{S}^{\alpha}_{\rm random}\sim\frac{D_\eta\Lambda}{2v_F}\sum_{\sigma,\sigma'}\sum_{\beta=1}^{N}\int\frac{d^d\mathbf{k}}{(2\pi)^d}\int\frac{d^d\mathbf{k}'}{(2\pi)^d}\prod_{i=1}^{4} \times\int_{-\infty}^{\infty}\frac{d\varepsilon_i}{2\pi}\delta(\varepsilon_4+\varepsilon_3-\varepsilon_2-\varepsilon_1)c_\sigma^{\alpha *}(\mathbf{k},\varepsilon_4) \times c_{\sigma'}^{\beta *}(\mathbf{k}',\varepsilon_3)c_{\sigma'}^{\beta}(\mathbf{k}',\varepsilon_2)c_\sigma^{\alpha}(\mathbf{k},\varepsilon_1) -\frac{D_\xi\Lambda}{2v_F}\sum_{\sigma,\sigma'}\sum_{\beta=1}^{N}\int\frac{d^d\mathbf{k}}{(2\pi)^d}\int\frac{d^d\mathbf{k}'}{(2\pi)^d}\prod_{i=1}^{4} \times\int_{-\infty}^{\infty}\frac{d\varepsilon_i}{2\pi}\delta(\varepsilon_4+\varepsilon_3-\varepsilon_2-\varepsilon_1) \tag{28}$$

$$c_\sigma^{\alpha *}(\mathbf{k}+\mathbf{Q},\varepsilon_4)c_{\sigma'}^{\beta *}(\mathbf{k}'-\mathbf{Q},\varepsilon_3)c_\sigma^{\alpha}(\mathbf{k},\varepsilon_2)c_{\sigma'}^{\beta}(\mathbf{k}',\varepsilon_1),$$

where

$$c_\sigma^{\alpha}(\mathbf{x},\tau)=T^{1/2}\sum_{\mathbf{k}}e^{i(\mathbf{k}\cdot\mathbf{x}-\varepsilon\tau)}c_\sigma^{\alpha}(\mathbf{k},\varepsilon). \tag{29}$$

The actions for the random scatterings inside the same replica [$\beta=\alpha$] are absorbed into the two-particle backward and forward scatterings by introducing[28]

$$\tilde{g}_1=g_1-\tilde{D}_\xi, \tag{30}$$

$$\tilde{g}_2=g_2-\tilde{D}_\eta, \tag{31}$$

where $\tilde{D}_\xi=D_\xi\Lambda/\pi v_F^2$ and $\tilde{D}_\eta=D_\eta\Lambda/\pi v_F^2$. Now, in addition to the two-particle scattering vertices [Figs. 1(a)–1(c)], there appear interreplica vertices as shown in Figs. 6(a) and 6(b).

B. One-loop renormalization

We obtain the vertex correction diagrams for $\tilde{g}_1$, $\tilde{g}_2$, and g_3 merely by replacing g_1 and g_2 in Fig. 2 with $\tilde{g}_1$ and $\tilde{g}_2$, respectively. However, we must avoid counting the diagram as shown in Fig. 6(c) which apparently renormalizes $\tilde{g}_1$, but vanishes in the replica limit, $N\to 0$, since summation over the replica indices $\gamma=1,2,\ldots,N$ of the inner loop yields N. Keeping this point in mind, we obtain the renormalized scattering strength, $\tilde{g}_1'$, $\tilde{g}_2'$, and g_3', which are analogous to Eqs. (11)–(13) and given by

$$\tilde{g}_1'=\tilde{g}_1+\tilde{g}_1\tilde{g}_2\ln\frac{\omega}{E_0}-[(\tilde{g}_2-\tilde{g}_1)\tilde{g}_1+\tilde{D}_\xi^2]\pi(\omega), \tag{32}$$

$$\tilde{g}_2'=\tilde{g}_2+\frac{1}{2}(\tilde{g}_1^2+\tilde{g}_2^2)\ln\frac{\omega}{E_0}-\frac{1}{2}(\tilde{g}_2^2+g_3^2)\pi(\omega), \tag{33}$$

$$g_3'=g_3+g_3(\tilde{g}_1-2\tilde{g}_2)\pi(\omega). \tag{34}$$

Renormalization of the interreplica vertices for $\beta\neq\alpha$ in Figs. 6(a) and 6(b) comes from the vertex correction diagrams as shown in Figs. 7(a) and 7(b), respectively. We must avoid counting the diagram Fig. 7(b-4) which vanishes in the replica limit. We obtain

$$\tilde{D}_\eta'=\tilde{D}_\eta-\frac{1}{2}\tilde{D}_\xi^2\ln\frac{\omega}{E_0}, \tag{35}$$

$$\tilde{D}_\xi'=\tilde{D}_\xi-\tilde{D}_\eta\tilde{D}_\xi\ln\frac{\omega}{E_0}+[(2\tilde{g}_1-\tilde{g}_2)\tilde{D}_\xi+2\tilde{D}_\xi^2]\pi(\omega). \tag{36}$$

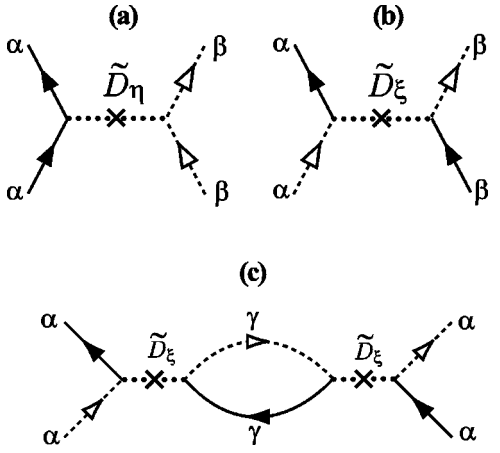

FIG. 6. Interreplica vertices originating from the random (a) forward and (b) backward scatterings. (c) The diagram that is proportional to the number of replicas N and vanishes in the replica limit $N\to 0$.

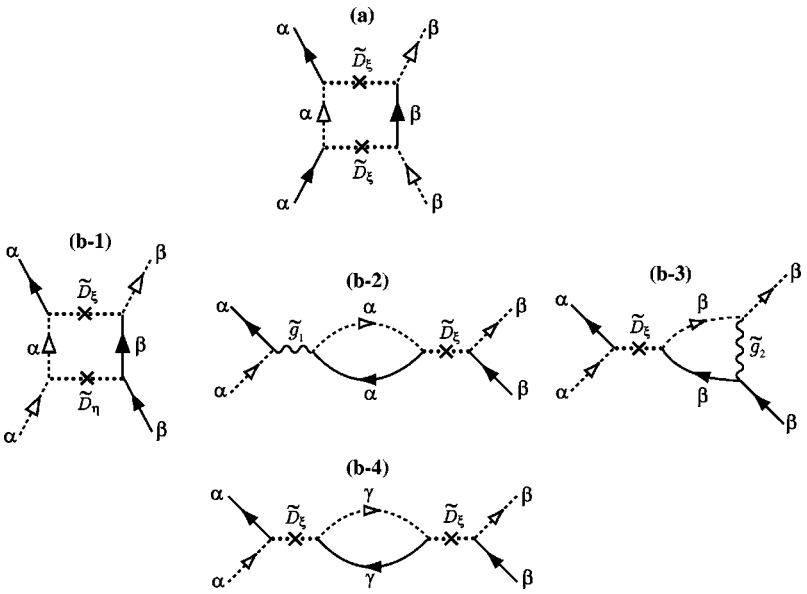

FIG. 7. The vertex correction diagrams for the interreplica (a) forward $[\tilde{D}_\eta]$ and (b) backward $[\tilde{D}_\xi]$ processes. We must avoid counting the diagram (b-4) which vanishes in the replica limit.

When we differentiate Eqs. (32)–(36) with respect to the scaling parameter, $l=\ln(E_0/\omega)$, the length scale Λ, must also be scaled in accordance with the change of the energy scale ω, as

$$\frac{d\Lambda}{\Lambda}+\frac{d\omega}{\omega}=0. \tag{37}$$

Thus we obtain the RG equations

$$\frac{d\tilde{g}_1}{dl}=-\tilde{D}_\xi-\tilde{g}_1\tilde{g}_2+[(\tilde{g}_2-\tilde{g}_1)\tilde{g}_1+\tilde{D}_\xi^2]\lambda_l, \tag{38}$$

$$\frac{d\tilde{g}_2}{dl}=-\tilde{D}_\eta-(\tilde{g}_1^2+\tilde{g}_2^2)/2+(\tilde{g}_2^2+g_3^2)\lambda_l/2, \tag{39}$$

$$\frac{dg_3}{dl}=-g_3(\tilde{g}_1-2\tilde{g}_2)\lambda_l, \tag{40}$$

$$\frac{d\tilde{D}_\eta}{dl}=\tilde{D}_\eta+\tilde{D}_\xi^2/2, \tag{41}$$

$$\frac{d\tilde{D}_\xi}{dl}=\tilde{D}_\xi+\tilde{D}_\xi\tilde{D}_\eta-[(2\tilde{g}_1-\tilde{g}_2)\tilde{D}_\xi+2\tilde{D}_\xi^2]\lambda_l. \tag{42}$$

C. Renormalization-group flow and QPT

1. In the absence of the random backward scattering

First, we consider the case where the random forward scattering is present ($\tilde{D}_{\eta;0}\neq 0$), but the random backward scattering is absent ($\tilde{D}_{\xi;0}=0$), where $\tilde{D}_{\eta;0}$ and $\tilde{D}_{\xi;0}$ are initial strengths of the random forward and backward scatterings, respectively. In this case, the RG flows indicate that the QPT occurs from a metallic fixed point ($\tilde{D}_\eta^*=\infty$, $g_3^*=0$) to the Mott insulator fixed point ($\tilde{D}_\eta^*=\infty$, $g_3^*=\infty$) as $\tilde{U}$ increases. Typical flows are shown in Figs. 8(a-1) and 8(a-2) for $\tilde{U}=0.1$ and 0.4, respectively, in the case of $d=1.1$ and $\tilde{D}_{\eta;0}=0.02$, where the critical value of $\tilde{U}$ is $\tilde{U}_c\sim 0.330$. This behavior in $d=1+\epsilon$ qualitatively reproduces the case of $d=1$,[18] where sufficiently strong random forward scattering destroys the Mott gap.

In Fig. 9(a) is shown a low-energy asymptotic phase diagram, where we also show energy scales of the Mott gap, $\omega_{\rm gap}/E_0$, introduced in the previous section. We see that both the random forward scattering and the raising dimensionality tend to destroy the Mott gap and consequently widen the metallic region as compared with the pure case (the phase boundary in the pure case is shown by the gray solid line).

2. Effects of the random backward scattering

Next, we consider the case where both the random forward and backward scatterings are present: $\tilde{D}_{\eta;0}\neq 0$ and $\tilde{D}_{\xi;0}\neq 0$. The random backward scattering makes it possible for the Anderson localization to occur. In this case, there occurs a transition from the Anderson insulator fixed point, ($\tilde{D}_\xi^*=\infty$, $\tilde{D}_\eta^*=\infty$, $g_3^*=0$), to the Mott insulator fixed point, ($\tilde{D}_\xi^*=\infty$, $\tilde{D}_\eta^*=\infty$, $g_3^*=\infty$), as $\tilde{U}$ increases. Typical flows are shown in Figs. 8(b-1) and 8(b-3) for $\tilde{U}=0.1$ and 0.4, respectively. We here introduce the scale $l_{\rm loc}$ at which $\tilde{D}_\xi$ reaches unity [see Fig. 8(b-1)]. Then, $\omega_{\rm loc}=E_0e^{-l_{\rm loc}}$ gives a qualitative energy scale around which a crossover to the Anderson insulator occurs. In the flows of the type of Fig. 8(b-3), g_3 always dominates $\tilde{D}_\xi$ and reaches unity at the scale $l=l_{\rm gap}<l_{\rm loc}$, indicating that the Mott gap formation overwhelms the Anderson localization.

We also find flows toward ($\tilde{D}_\xi^*=0$, $\tilde{D}_\eta^*=\infty$, $g_3^*=0$), as shown in Fig. 8(b-2). This type of flow is found only for $0<d<1.575$ in the narrow region of $\tilde{U}$ in between the regions corresponding to Figs. 8(b-1) and 8(b-3). In these cases, however, $\tilde{D}_\xi$ exceeds unity at some scaling parameter $l_{\rm loc}$ during the renormalization, which indicates that the perturbative treatment breaks down and the localization occurs around the energy scale specified by $l=l_{\rm loc}$. Thus we interpret that the ground state corresponding to this fixed point is the Anderson insulator. It is beyond the RG-based scheme to

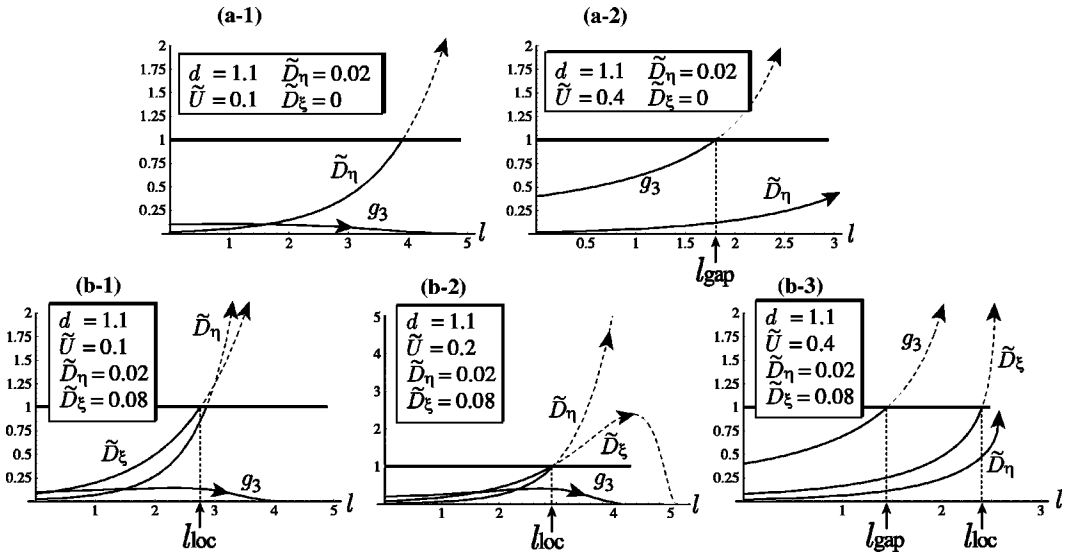

FIG. 8. (a) RG flows of $\tilde{D}_\eta$ and g_3 for (a-1) $\tilde{U}=0.1$ and (a-2) $\tilde{U}=0.4$ in the case of $d=1.1$, $\tilde{D}_{\eta;0}=0.02$, and $\tilde{D}_{\xi;0}=0$. (b) RG flows of $\tilde{D}_\eta$, $\tilde{D}_\xi$, and g_3 for (b-1) $\tilde{U}=0.1$, (b-2) $\tilde{U}=0.2$, and (b-3) $\tilde{U}=0.4$ in the case of $d=1.1$, $\tilde{D}_{\eta;0}=0.02$, and $\tilde{D}_{\xi;0}=0.08$.

settle this ambiguity and we do not go into the details on this issue here.

In Fig. 9(b) is shown a low-energy asymptotic phase diagram, where we also show $\omega_{\rm loc}/E_0$ and $\omega_{\rm gap}/E_0$. As compared with Fig. 9(a), the phase boundary remains nearly unchanged, but the metallic phase in Fig. 9(a) is replaced with the Anderson insulator phase due to the random backward scattering.

The present results indicate that the QPT from the Anderson to the Mott insulators occurs in both $d=1$ and $d>1$. Recently, Ohtsuka and Hatsugai[20] studied the half-filled Hubbard model containing site randomness by using the Monte Carlo method. They found that the QPT's from an incompressible (Mott) to a compressible (Anderson) insulator occur in all the cases of $d=1, 2, 3$. This numerical result is consistent with the RG-based views given here.

IV. CONCLUDING REMARKS

In this paper, based on the one-loop RG flows, we have studied QPT's in the Hubbard model with a circular Fermi surface in $d=1+\epsilon$ continuous dimensions, where we assume that there is $2k_F$ umklapp scattering present *a priori*. Peculiarity of the $d=1+\epsilon$ dimensions was incorporated only through the mathematical structure of the elementary PP and PH loops: infrared logarithmic singularity of the PH loop is smeared. We have studied the following three cases:

(1) *In the absence of randomness*: The QPT from the metallic phase to the Mott insulator phase occurs at a finite U for $\epsilon>0$.

(2) *In the case where the random forward scattering is present, but the random backward scattering is absent*: Both random forward scattering and raising dimensionality tend to destroy the Mott gap. Consequently, $\tilde{U}_c$ becomes finite for $\epsilon\geqslant 0$ and the metallic region becomes wider as compared with the pure case (1).

(3) *In the case where both the random forward and backward scatterings are present*: The phase boundary remains nearly unchanged as compared with the case (2), but the metallic phase in the case (2) is replaced with the Anderson insulator phase due to the random backward scattering.

In the present paper, the ground-state properties were conjectured based solely on the one-loop RG flows. At present, numerical studies are in progress to complement the views given here.[30]

ACKNOWLEDGMENTS

The author acknowledges Professor K. Ueda for directing his attention to Ref. 16. He also thanks Professors K. Yonemitsu and Y. Hatsugai for discussions and useful information. He was supported by a Grant-in-Aid for Encouragement of Young Scientists from the Ministry of Education, Science, Sports, and Culture, Japan.

APPENDIX A: DERIVATION OF EQ. (10)

Our purpose here is to show that the $\tilde{\omega}$ dependence of $\Re\,\Pi_{2k_F}(\omega)$ is uniquely determined as Eq. (10). We start with Eq. (9). The imaginary counterpart is given by

$$\Im\,\Pi_{2k_F}(\omega)=-\pi\frac{S_{d-1}}{(2\pi)^d}\int k^{d-1}dk\int_0^\pi d\theta(\sin\theta)^{d-2}\times\Theta(-\xi_{\boldsymbol{k}})\Theta(\xi_{\boldsymbol{k}+\boldsymbol{Q}})\,\delta(\omega-\xi_{\boldsymbol{k}+\boldsymbol{Q}}+\xi_{\boldsymbol{k}}) \quad \text{(A1)}$$

for $0<\omega<2v_Fk_F$, $\Im\,\Pi_{2k_F}(\omega)=0$ for $2v_Fk_F<\omega$, and satisfies $\Im\,\Pi_{2k_F}(-\omega)=-\Im\,\Pi_{2k_F}(\omega)$. The delta function in the integrand of Eq. (A1) is rewritten as

$$\delta(\omega-\xi_{\boldsymbol{k}+\boldsymbol{q}}+\xi_{\boldsymbol{k}})=\frac{1}{v_Fk_F}\left(\frac{1}{2}+\frac{\tilde{\omega}}{\tilde{k}}\right)\delta(t-t_0),$$

where we introduced $\tilde{\omega}=\omega/2v_Fk_F$, $\tilde{k}=k/k_F$, $t=\cos\theta$, and $t_0=\tilde{\omega}-(1-\tilde{\omega}^2)/\tilde{k}$. So we have

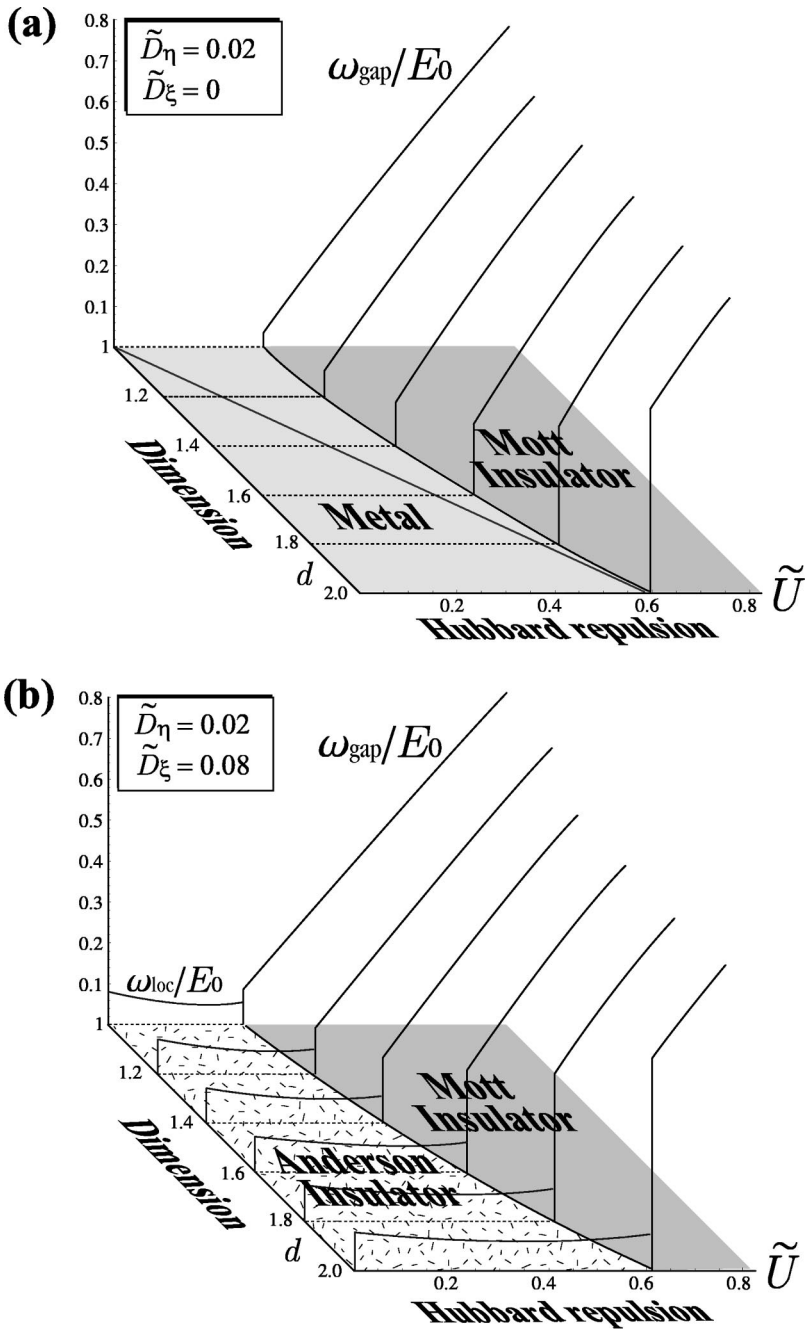

FIG. 9. Low-energy asymptotic phase diagrams in the cases where (a) the random forward scattering is present, but the random backward scattering is absent, and (b) both the random forward and backward scatterings are present. In (a), the phase boundary in the pure case (see Fig. 5) is shown by the gray solid line. We also show $\omega_{\rm loc}/E_0$ and $\omega_{\rm gap}/E_0$, as a function of d and $\tilde{U}$.

$$\Im\Pi_{2k_F}(\omega) = -\pi \frac{S_{d-1}k_F^{d-1}}{(2\pi)^d v_F} \int_{1-\tilde{\omega}}^{1} d\tilde{k} \left(\frac{1}{2} + \frac{\tilde{\omega}}{\tilde{k}}\right) \tilde{k}^{d-1} \times \left[1 - \left(\tilde{\omega} - \frac{1-\tilde{\omega}^2}{\tilde{k}}\right)^2\right]^{(d-3)/2}$$
$$= -\pi \frac{S_{d-1}k_F^{d-1}}{2(2\pi)^d v_F} (1-\tilde{\omega}^2)^{(d-3)/2} \times \int_1^{1+\tilde{\omega}} du (u^2-\tilde{\omega}^2)(u^2-1)^{(d-3)/2}, \quad \text{(A2)}$$

where $u = \tilde{k} + \tilde{\omega}$. For small $\tilde{\omega}$, since the region of integration is limited to the vicinity of $u=1$, it is reasonable to replace the integrand, $(u^2-\tilde{\omega}^2)(u^2-1)^{(d-3)/2}$, with $2^{(d-3)/2}(u-1)^{(d-3)/2}$ and we have

$$\Im\Pi_{2k_F}(\omega) \sim -\pi \frac{S_{d-1}k_F^{d-1}}{2(2\pi)^d v_F} 2^{(d-3)/2} \times (1-\tilde{\omega}^2)^{(d-3)/2} \int_1^{1+\tilde{\omega}} du (u-1)^{(d-3)/2}$$
$$= -\pi \frac{S_{d-1}k_F^{d-1}}{2(2\pi)^d v_F} \frac{2^{(d-1)/2}}{d-1} \times (1-\tilde{\omega}^2)^{(d-3)/2} \tilde{\omega}^{(d-1)/2}, \quad \text{(A3)}$$

which corresponds to a special case of Eq. (7.12) in Ref. 17 for $|\boldsymbol{q}| = 2k_F$. In $d = 1+\epsilon$, noting $S_{d-1} \sim \epsilon$, we obtain

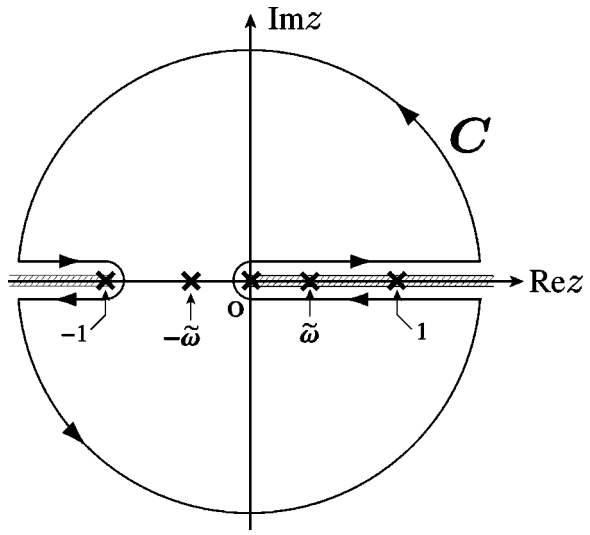

FIG. 10. Contour to evaluate the integral (A6).

$$\Im\Pi_{2k_F}(\omega)\sim-\frac{1}{4v_F}(1-\tilde{\omega}^2)^{-1+\epsilon/2}\tilde{\omega}^{\epsilon/2}. \tag{A4}$$

The real counterpart is obtained by the Kramers-Kronig transformation,

$$\Re\Pi_{2k_F}(\omega)=\frac{2}{\pi}\mathcal{P}\int_0^1 d\tilde{\omega}'\frac{\tilde{\omega}'\Im\Pi_{2k_F}(\omega')}{\tilde{\omega}'^2-\tilde{\omega}^2}, \tag{A5}$$

where the symbol $\mathcal{P}$ denotes Cauchy principal value integral (note that $0<\tilde{\omega}<1$). Since the prefactor $(1-\tilde{\omega}^2)^{-1+\epsilon/2}$ on the right-hand side of Eq. (A4) has already appeared in the exact expression (A2), and the remaining part of the integral, Eq. (A2), shows no singularity at $\tilde{\omega}=1$, the expression for small $\tilde{\omega}$, Eq. (A4), holds analytical property of $\Im\Pi_{2k_F}(\omega)$ correctly even for $\tilde{\omega}\sim1$. Thus it is reasonable to use expression (A4) in Eq. (A5) and we have

$$\Re\Pi_{2k_F}(\omega)\sim-\frac{1}{2\pi v_F}\mathcal{P}\int_0^1 d\tilde{\omega}'\frac{\tilde{\omega}'^{1+\epsilon/2}}{(\tilde{\omega}'^2-\tilde{\omega}^2)(1-\tilde{\omega}'^2)^{1-\epsilon/2}}, \tag{A6}$$

which is to be evaluated for small $\tilde{\omega}$ and ϵ.

To evaluate Eq. (A6), let

$$f(z)=\frac{z}{(z^2-\tilde{\omega}^2)(z^2-1)}[z(z^2-1)]^{\epsilon/2}, \tag{A7}$$

and consider the integral

$$\oint_C f(z)dz$$

along the contour as depicted in Fig. 10. $f(z)$ has poles at $z=\pm\tilde{\omega}$ and branch points at $z=0,\infty$ and $z=\pm1$. We choose branch cuts in the region $\{\Re z<-1\}\cup\{0<\Re z\}$. In the limit as the large circle recedes to infinity, it gives no contribution. The residue at the pole $z=-\tilde{\omega}$ gives

$$\oint_C f(z)dz=-\pi i e^{\pi i\epsilon/2}\frac{\tilde{\omega}^{\epsilon/2}}{(1-\tilde{\omega}^2)^{1-\epsilon/2}}\sim-\pi i\tilde{\omega}^{\epsilon/2}. \tag{A8}$$

The remainder of the contour is deformed into an integral enclosing the cuts and encircling the pole $z=\tilde{\omega}$ and the branch points at $z=0$ and $z=\pm1$. The points $z=0,\pm1$ give no contribution. The integrals encircling the pole $z=\tilde{\omega}$ and the remainder along the real axis give

$$\begin{aligned}\oint_C f(z)dz=&\frac{\pi i}{2}(e^{(\pi/2)i\epsilon}+e^{(3\pi/2)i\epsilon})\frac{\tilde{\omega}^{\epsilon/2}}{(1-\tilde{\omega}^2)^{1-\epsilon/2}}\\&+2\pi v_F(e^{(\pi/2)i\epsilon}-e^{(3\pi/2)i\epsilon})\Re\Pi_{2k_F}(\omega)\\&+(e^{(4\pi/2)i\epsilon}-1)\int_1^\infty\frac{x[x(x^2-1)]^{\epsilon/2}}{(x^2-\tilde{\omega}^2)(x^2-1)}dx\\&+(e^{(3\pi/2)i\epsilon}-e^{(\pi/2)i\epsilon})\\&\times\int_{-\infty}^{-1}\frac{x[-x(x^2-1)]^{\epsilon/2}}{(x^2-\tilde{\omega}^2)(x^2-1)}dx.\end{aligned}$$

Here the integrals are evaluated for small $\tilde{\omega}$ and ϵ as

$$\begin{aligned}\int_1^\infty\frac{x[x(x^2-1)]^{\epsilon/2}}{(x^2-\tilde{\omega}^2)(x^2-1)}dx&=-\int_{-\infty}^{-1}\frac{x[-x(x^2-1)]^{\epsilon/2}}{(x^2-\tilde{\omega}^2)(x^2-1)}dx\\&\sim\int_1^\infty[x(x^2-1)]^{-1+\epsilon/2}dx\\&=\frac{\Gamma(1-3\epsilon/4)\Gamma(\epsilon/2)}{2\Gamma(1-\epsilon/2)}\sim1/\epsilon,\end{aligned}$$

where the integral in the second line converges for $0<\epsilon<4/3$. We thus obtain, for small $\tilde{\omega}$ and ϵ,

$$\oint_C f(z)dz=\pi i\tilde{\omega}^{\epsilon/2}-2\pi^2 v_F i\epsilon\,\Re\Pi_{2k_F}(\omega)+2\pi i-\pi i. \tag{A9}$$

Therefore, we obtain $\Re\Pi_{2k_F}(\omega)$ of the form that is correct up to the leading order of $\tilde{\omega}$,

$$\Re\Pi_{2k_F}(\omega)\sim\frac{1}{2\pi v_F}\left[\frac{\tilde{\omega}^{\epsilon/2}}{\epsilon/2}+C_\epsilon\right], \tag{A10}$$

which is Eq. (10). Although above manipulation gives $C_\epsilon=1/\epsilon$, it seems feasible to choose $C_\epsilon=-2/\epsilon$ as suggested in Ref. 16 to reproduce correctly the limit form of $\Re\Pi_{2k_F}(\omega)=(1/2\pi v_F)\log\tilde{\omega}$ at $\epsilon=0$. This discrepancy may arise, because to evaluate Eq. (A5) we used expression (A4) which holds analytical property of $\Im\Pi_{2k_F}(\omega)$ correctly but misses contribution from $\tilde{\omega}\sim1$. We do not go into the details here, since an explicit form of C_ϵ does not enter the RG equations (15)–(17) and (38)–(42).

*Email: kishine@ims.ac.jp

[1] See M. Imada, A. Fujimori, and Y. Tokura, Rev. Mod. Phys. **70**, 1039 (1998) and references therein.
[2] E.H. Lieb and F.Y. Wu, Phys. Rev. Lett. **20**, 1445 (1968).
[3] J.E. Hirsh, Phys. Rev. B **31**, 4403 (1985).
[4] H.Q. Lin and J.E. Hirsh, Phys. Rev. B **35**, 3359 (1987).
[5] H. Kondo and T. Moriya, J. Phys. Soc. Jpn. **65**, 2559 (1996).
[6] W. Metzner and D. Vollhardt, Phys. Rev. Lett. **62**, 324 (1989).
[7] A. Georges, G. Kotliar, W. Krauth, and M.J. Rozenberg, Rev. Mod. Phys. **68**, 13 (1996).
[8] M. Kimura, Prog. Theor. Phys. **53**, 955 (1975).
[9] J. Sólyom, Adv. Phys. **28**, 201 (1979).
[10] V.J. Emery, R. Bruinsma, and S. Barisic, Phys. Rev. Lett. **48**, 1039 (1982).
[11] K. Yonemitsu, Phys. Rev. B **56**, 7262 (1997).
[12] C. Bourbonnais, J. Phys. I **3**, 143 (1993).
[13] Y. Suzumura, M. Tsuchiizu, and G. Grüner, Phys. Rev. B **57**, 15 040 (1998).
[14] J. Kishine and K. Yonemitsu, J. Phys. Soc. Jpn. **68**, 2790 (1999).
[15] S. Fujimoto, preprint, cond-mat/9910069 (unpublished).
[16] K. Ueda and T.M. Rice, Phys. Rev. B **29**, 1514 (1984).
[17] The elementary PP and PH loops in general d dimensions are extensively discussed in Chap. 7 of W. Metzner, C. Castellani, and C.D. Castro, Adv. Phys. **47**, 317 (1998).
[18] S. Fujimoto and N. Kawakami, Phys. Rev. B **54**, 11 018 (1996).
[19] Y. Otsuka, Y. Morita, and Y. Hatsugai, Phys. Rev. B **58**, 15 314 (1998).
[20] Y. Otsuka and Y. Hatsugai (preprint).
[21] W. Metzner and C. Di Castro, Phys. Rev. B **47**, 16 107 (1993).
[22] K.G. Wilson, Phys. Rev. Lett. **28**, 548 (1972).
[23] P.B. Weigmann, J. Phys. C **11**, 1583 (1978); J.B. Kogut, Rev. Mod. Phys. **55**, 775 (1983).
[24] K. Yonemitsu, Mol. Cryst. Liq. Cryst. (to be published).
[25] The RG-based discussion on the magnitude of the gap in the $d=1$ attractive ($U<0$) Hubbard model is found in A.I. Larkin and J. Sak, Phys. Rev. Lett. **39**, 1025 (1977).
[26] See M. Takahashi, *Thermodynamics of One-Dimensional Solvable Models* (Cambridge University Press, Cambridge, 1999), Sec. 6.5.
[27] Interplay of the correlation and randomness in $d=1$ is extensively reviewed in T. Saso, Y. Suzumura, and H. Fukuyama, Prog. Theor. Phys. Suppl. **84**, 269 (1985).
[28] T. Giamarchi and H.J. Schulz, Phys. Rev. B **37**, 325 (1988).
[29] D. Belitz and T.R. Kirkpatrick, Rev. Mod. Phys. **66**, 261 (1994).
[30] K. Yonemitsu and J. Kishine, J. Phys. Soc. Jpn. (to be published).